

See discussions, stats, and author profiles for this publication at: <https://www.researchgate.net/publication/11062868>

New Iron(III) Phosphate Phases: Crystal Structure and Electrochemical and Magnetic Properties

ARTICLE *in* INORGANIC CHEMISTRY · NOVEMBER 2002

Impact Factor: 4.76 · DOI: 10.1002/chin.200304024 · Source: PubMed

CITATIONS

63

READS

219

4 AUTHORS, INCLUDING:



[Peter Y. Zavalij](#)

University of Maryland, College Park

434 PUBLICATIONS 8,165 CITATIONS

SEE PROFILE



[Masatsugu Sei Suzuki](#)

Binghamton University

245 PUBLICATIONS 1,531 CITATIONS

SEE PROFILE

New Iron(III) Phosphate Phases: Crystal Structure and Electrochemical and Magnetic Properties

Yanning Song,[†] Peter Y. Zavalij,[†] Masatsugu Suzuki,[‡] and M. Stanley Whittingham^{*,†}

Departments of Chemistry and Physics and Institute for Materials Research, State University of New York at Binghamton, Binghamton, New York 13902-6016

Received April 30, 2002

Two new iron(III) phosphates, FePO_4 , have been synthesized from the dehydration of hydrothermally prepared monoclinic and orthorhombic hydrated phosphates $\text{FePO}_4 \cdot 2\text{H}_2\text{O}$. The structures of both hydrates were redetermined from single crystal data. On dehydration, a topotactic reaction takes place with only those bonds associated with the water molecules being broken, so that both FePO_4 phases have essentially the same Fe–P backbone frameworks as the corresponding hydrates. They are, respectively, monoclinic FePO_4 , space group $P2_1/n$, $a = 5.480(1) \text{ \AA}$, $b = 7.480(1) \text{ \AA}$, $c = 8.054(1) \text{ \AA}$, $\beta = 95.71(1)^\circ$, and $Z = 4$; and orthorhombic FePO_4 , space group $Pbca$, $a = 9.171(1) \text{ \AA}$, $b = 9.456(1) \text{ \AA}$, $c = 8.675(1) \text{ \AA}$, and $Z = 8$. Both of these phases are thermally unstable relative to the trigonal quartz-like FePO_4 . The electrochemical studies find that the orthorhombic iron phosphate is more active than the monoclinic phase, while both are more active than trigonal FePO_4 . Both phases approach Curie–Weiss behavior at room temperature, with the monoclinic phase exhibiting stronger antiferromagnetic interactions due to Fe–O–Fe interactions. The electrochemical and magnetic data are consistent with the structures of these two compounds. The properties of these new iron phosphate structures are compared with other iron phosphate phases.

Introduction

Iron phosphate, FePO_4 , has long been used in the steel¹ and glass² industries. It has recently been proposed as the cathode^{3,4} in lithium batteries, and lithium metal phosphates can be used as either cathode⁵ or anode⁶ in lithium batteries. At normal pressures, it adopts a verlinite (AlPO_4) structure related to α -quartz with each iron and phosphorus atom tetrahedrally bonded to four oxygen atoms.⁷ Kinomura et al.⁸ found that at 5 GPa FePO_4 takes up the CrVO_4 -type

structure, which has the iron in octahedral coordination and has a 23% higher density than the verlinite form. An amorphous phase has also been reported⁹ to be present at 2.5 GPa. The existence of the amorphous phase was confirmed by Raman scattering and Mossbauer spectroscopy. On extracting lithium from LiFePO_4 , the orthorhombic heterosite FePO_4 with $a = 9.8142(2) \text{ \AA}$, $b = 5.7893(2) \text{ \AA}$, and $c = 4.7820(2) \text{ \AA}$ is obtained;¹⁰ this phase which contains FeO_6 octahedra converts to the trigonal verlinite phase on heating.¹¹ This phase in turn on extensive heating converts partially into an amorphous phase.¹²

Iron phosphates have also been reported as good catalysts for selective oxidation reactions,¹³ being particularly effective

* Corresponding author. Phone: +1-607-777-4623. E-mail: stanwhit@binghamton.edu.

[†] Department of Chemistry and Institute for Materials Research.

[‡] Department of Physics and Institute for Materials Research.

- (1) Boras, C. A.; Romagnoli, R.; Lezna, R. O. *Electrochim. Acta* **2000**, *45*, 1717–1725.
- (2) Mogus-Milankovic, A.; Day, D. E.; Long, G. J.; Marasinghe, G. K. *Phys. Chem. Glasses* **1996**, *37*, 57–61.
- (3) Prosini, P. P.; Lisi, M.; Scaccia, S.; Carewska, M.; Cardelline, F.; Pasquali, M. *J. Electrochem. Soc.* **2002**, *149*, A297–A301.
- (4) Song, Y.; Yang, S.; Zavalij, P. Y.; Whittingham, M. S. *Mater. Res. Bull.* **2002**, *37*, 1249–1257.
- (5) Padhi, A. K.; Nanjundaswamy, K. S.; Goodenough, J. B. *J. Electrochem. Soc.* **1997**, *144*, 1188–1194.
- (6) Chen, J.-M.; Li, Y. J.; Hurng, W.-M.; Whittingham, M. S. (Industrial Technology Research Institute, Chutung, Taiwan). Secondary Lithium Battery using a New Layered Anode Material. U.S. Patent 5,514,490, 1996.
- (7) Ng, H. N.; Calvo, C. *Can. J. Chem.* **1975**, *53*, 2064–2067.

- (8) Kinomura, N.; Shimada, M.; Koizumi, M. *Mater. Res. Bull.* **1976**, *11*, 457–460.
- (9) Pasternak, M. P.; Rozenberg, G. K.; Milner, A. P.; Amanowicz, M.; Schwaes, U.; Syassen, K.; Taylor, R. D.; Hanfland, M.; Brister, K. *Phys. Rev. Lett.* **1997**, *79*, 4409–4412. Pasternak, M. P.; Rozenberg, G. K.; Milner, A. P.; Amanowicz, M.; Brister, K. E.; Taylor, R. D. *J. Magn. Magn. Mater.* **1998**, *183*, 185–187.
- (10) Andersson, A. S.; Kalska, B.; Haggstrom, L.; Thomas, J. O. *Solid State Ionics* **2000**, *130*, 41–52.
- (11) Yang, S.; Song, Y.; Zavalij, P.; Whittingham, M. S. *Electrochem. Commun.* **2002**, *4*, 239–244.
- (12) Long, C. J.; Cheetham, A. K.; Battle, P. D. *Inorg. Chem.* **1983**, *22*, 3012–3016. Battle, P. D.; Gibb, T. C.; Hu, G.; Munro, D. C.; Attfield, J. P. *J. Solid State Chem.* **1986**, *65*, 343–350.

for oxidative dehydrogenation but not for an oxygen insertion reaction in compounds such as isobutyric acid,¹⁴ lactic acid,¹⁵ and glycolic acid.¹⁶ At the same time, the widespread applications of open-framework inorganic materials in heterogeneous catalysis, separations, and ion exchange processes¹⁷ have stimulated extensive studies on the incorporation of other cations and/or anions into the FePO₄ structures. The combination of potentially interesting magnetic properties and the sieving properties of these open-framework phosphates has opened the new way to a new class of porous materials. Several new compounds in the iron(III) families have recently been synthesized,^{18–21} and their properties have been recently reviewed by Cavellec et al.²² Kinomura et al.⁸ showed that α -quartz and CrVO₄-type FePO₄ are high spin ferric exhibiting Curie–Weiss behavior. Bruckner et al.^{23,24} found, from Mossbauer effect studies, that α -quartz FePO₄ is antiferromagnetic below ca. 25 K. Long et al.¹² found that it undergoes a spin-reorientation transition at ca. 17 K.

We report here the synthesis, crystal structure, and magnetic and electrochemical properties of two new iron(III) phosphates. Their structures are closely related to those of the hydrated compounds from which they were formed, but they differ significantly from the known heterosite and verlinite forms where the iron coordination is octahedral and tetrahedral, respectively.

Experimental Section

Synthesis. FePO₄·2H₂O was hydrothermally synthesized from a mixture of FeCl₂ (Aldrich), LiCl (Fisher), and standardized 1.85 M H₃PO₄; 0.02 mol of each were added to 1.3 mol of water. The mixture was sealed in a 125 mL Parr Teflon-lined stainless steel autoclave and heated at 145–170 °C for 4–12 h. For reaction times longer than 8 h, only polycrystalline monoclinic FePO₄·2H₂O (phosphosiderite) (**A**) is obtained. The purity was shown by powder X-ray diffraction and thermal gravimetric analysis (TGA). For shorter reaction times, with an initial pH of 0.57, a mixture of phosphosiderite and orthorhombic FePO₄·2H₂O (strengite) (**B**) single crystals was obtained. These large 0.25 mm³ crystals of **B** were easily separated from the other green powder products.

Crystals of **A** and **B** were heated at 80 °C in a vacuum oven for 12 h. The corresponding dehydrated iron phosphates **C** and **D** were obtained. Thermal analysis in nitrogen at 5 °C/min on a Perkin-Elmer TGA showed that there is no water in these compounds, and chemical analysis showed that the Fe/P ratio was unity.

Magnetic Measurements. The temperature-dependent dc magnetic susceptibility was measured using a Quantum Design MPMS

Table 1. Crystallographic Data for Monoclinic (**A**) and Orthorhombic (**B**) FePO₄·2H₂O, and Monoclinic (**C**) and Orthorhombic (**D**) FePO₄

	A	B	C^a	D
formula	FePO ₄ ·2H ₂ O	FePO ₄ ·2H ₂ O	FePO ₄	FePO ₄
fw	186.85	186.85	150.82	150.82
cryst syst	monoclinic	orthorhombic	monoclinic	orthorhombic
space group	<i>P</i> 2 ₁ / <i>n</i>	<i>Pbca</i>	<i>P</i> 2 ₁ / <i>n</i>	<i>Pbca</i>
<i>a</i> , Å	5.3071(10)	9.8674(11)	5.4802(6)	9.1708(12)
<i>b</i> , Å	9.7548(19)	10.0973(11)	7.4802(8)	9.4564(12)
<i>c</i> , Å	8.6752(16)	8.7046(10)	8.0537(10)	8.6753(11)
β , deg	90.163(4)		95.708(9)	
<i>V</i> , Å ³	449.11(15)	867.27(17)	328.51(12)	752.35(17)
<i>Z</i>	4	8	4	8
<i>D</i> _{calcd} , g·cm ^{−3}	2.763	2.862	3.049	2.663
μ , cm ^{−1}	3.649	3.780	5.01	4.285
<i>R</i> _{eq}	0.0427	0.0394	–	0.0344
<i>R</i> _{int}	0.0610	0.0234	0.0205 ^a	0.0297
<i>R</i> _{F2^{a,b}}				
<i>R</i> _{1^c} (<i>I</i> > 2 σ <i>I</i>)	0.0410	0.0252	0.0321 ^a	0.0783
<i>R</i> _{prof^{d,d}}				
w <i>R</i> _{2^e}	0.0953	0.0692	0.0516 ^a	0.1884
w <i>R</i> _{prof^{a,f}}				

^a Powder data. ^b $R_{F2} = \sum |F_o|^2 - F_c^2 / \sum |F_o|^2$. ^c $R_1 = \sum ||F_o| - |F_c|| / \sum |F_o|$. ^d $R_{prof} = \sum |Y_o - Y_c| / \sum Y_o$. ^e $wR_2 = [\sum w(F_o^2 - F_c^2)^2 / \sum w(F_o^2)^2]^{1/2}$. ^f $wR_{prof} = [\sum w(Y_o - Y_c)^2 / \sum wY_c^2]^{1/2}$.

XL SQUID magnetometer in a magnetic field of 1000 Oe over the temperature range 2–298 K with a 2 K step.

Redox Measurements. Electrochemical studies were conducted in a helium-filled glovebox using a Macpile galvanostat. The iron phosphate was mixed with 20 wt % carbon black and 10 wt % PTFE powder; around 20 mg/cm² was hot-pressed into a stainless steel Exmet grid for 1 h at about 120 °C. A bag cell configuration was used with a 1 M solution of LiPF₆ in 1:1 DEC/EC (EMI, LP40) as the electrolyte, pure lithium as the anode, and Celgard 2400 (Hoechst Celanese Corp.) for the separator.

X-ray Analysis. Powder diffraction patterns were obtained on a Scintag XDS2000 θ – θ powder diffractometer equipped with a Ge(Li) solid state detector (Cu K α radiation), on a Philips X'Pert-MPD diffractometer using a variable temperature stage from room temperature to 400 °C, and for Rietveld refinement on material **C** on a Rigaku rotating anode TTRAX diffractometer at room temperature in the range from 5° to 50° 2 θ with step 0.01° using Mo K α radiation. Single crystal studies on compounds **A**, **B**, and **D** were performed on a Bruker Smart Apex diffractometer at room temperature (Mo K α radiation, graphite monochromator). For these samples, a full reciprocal sphere was scanned, and integral intensities were corrected for absorption effect using SADABS software.²⁵

Crystal Structure Determination

Single Crystal Data. The structures of the monoclinic and orthorhombic hydrates **A** and **B** were previously determined from powder data^{26,27} but with low accuracy. Therefore, their crystal structures were redetermined from single crystal data (Table 1). The hydrogen atoms in both structures were located among the first peaks on the differential Fourier synthesis and refined to an O–H distance of 0.8 Å.

The structure of the new orthorhombic phosphate **D** was solved by direct methods²⁸ also from single crystal data. Crystals of **D** were obtained from orthorhombic **B** by solid state decomposition

- (13) Ai, M.; Ohdan, K. *J. Mol. Catal. A: Chem.* **2000**, *159*, 19–24.
- (14) Atkins, W. C. U.S. Patent 3,855,279.
- (15) Ai, M.; Ohdan, K. *Appl. Catal., A* **1997**, *150*, 13–20.
- (16) Ai, M.; Ohdan, K. *Stud. Surf. Sci. Catal.* **1997**, *110*, 527–534.
- (17) Ferey, G.; Cheetham, A. K. *Science* **1999**, *283*, 1125–1126.
- (18) Debord, J. R. D.; Reiff, W. M.; Warren, C. J.; Haushalter, R. C.; Zubieta, J. *Chem. Mater.* **1997**, *9*, 1994–1998.
- (19) Debord, J. R. D.; Reiff, W. M.; Haushalter, R. C.; Zubieta, J. *J. Solid State Chem.* **1996**, *125*, 186–191.
- (20) Cavellec, M.; Riou, D.; Ferey, G. *J. Solid State Chem.* **1994**, *112*, 441–442.
- (21) Lii, K.-H.; Huang, Y.-F. *Chem. Commun.* **1997**, 839–840.
- (22) Cavellec, M.; Riou, D.; Ferey, G. *Inorg. Chim. Acta* **1999**, *291*, 317–325.
- (23) Bruckner, W.; Fuchs, W.; Ritter, G. *Phys. Lett.* **1967**, *A26*, 32.
- (24) Beckmann, V.; Bruckner, W.; Fuchs, W.; Ritter, G.; Wegener, H. *Phys. Status Solidi* **1968**, *29*, 781.

- (25) Sheldrick, G. M. *SADABS*; University of Göttingen: Göttingen, Germany, 1996.
- (26) Moore, P. B. *Am. Mineral.* **1966**, *51*, 168.
- (27) Gay, H. D. *Rev. Asoc. Geol. Argent.* **1968**, *23*, 279.
- (28) Sheldrick, G. M. *Acta Crystallogr.* **1990**, *A46*, 467–473.

Table 2. Atomic Coordinates and Equivalent Isotropic Displacement Parameters for A–D

atom	x	y	z	$U_{eq}, \text{\AA}^2$
A, Monoclinic $\text{FePO}_4 \cdot 2\text{H}_2\text{O}$				
Fe1	0.0914(2)	0.67394(6)	0.69157(9)	0.0122(2)
P1	−0.0870(2)	0.3509(1)	0.6839(2)	0.0119(3)
O1	−0.1164(6)	0.5068(3)	0.6700(4)	0.0155(7)
O2	0.1659(6)	0.3221(3)	0.7638(4)	0.0171(8)
O3	−0.0944(7)	0.2814(4)	0.5268(4)	0.0193(8)
O4	−0.3002(6)	0.2937(4)	0.7831(4)	0.0168(8)
O5	0.0885(9)	0.6345(4)	0.9260(5)	0.0279(9)
O6	0.3924(7)	0.5489(4)	0.6816(6)	0.033(1)
B, Orthorhombic $\text{FePO}_4 \cdot 2\text{H}_2\text{O}$				
Fe1	0.32921(3)	0.36715(3)	0.15156(3)	0.0089(1)
P1	0.64554(5)	0.35158(5)	0.03174(6)	0.0080(1)
O1	0.4905(1)	0.3515(1)	0.0155(2)	0.0110(3)
O2	0.1797(1)	0.3891(2)	0.3017(2)	0.0131(3)
O3	0.2051(2)	0.2841(1)	0.0068(2)	0.0122(3)
O4	0.2936(2)	0.5471(1)	0.0810(2)	0.0134(3)
O5	0.4468(2)	0.4396(2)	0.3351(2)	0.0175(3)
O6	0.3889(2)	0.1875(2)	0.2348(2)	0.0145(3)
C, Monoclinic FePO_4				
Fe1	0.3881(5)	0.8059(4)	0.0602(3)	0.0126(3)
P1	0.5896(9)	0.4579(5)	0.2659(6)	0.0126(3)
O1	0.481(1)	0.640(1)	0.228(1)	0.0126(3)
O2	0.828(2)	0.463(1)	0.384(1)	0.0126(3)
O3	0.641(1)	0.358(1)	0.116(1)	0.0126(3)
O4	0.410(2)	0.343(1)	0.368(1)	0.0126(3)
D, Orthorhombic FePO_4				
Fe1	0.3995(2)	0.5645(2)	0.2841(2)	0.0233(5)
P1	0.1764(3)	0.3794(3)	0.1168(3)	0.0223(7)
O1	0.3190(9)	0.3929(10)	0.1914(9)	0.030(2)
O2	0.1065(10)	0.2270(10)	0.1558(10)	0.034(2)
O3	0.0820(9)	0.5157(9)	0.1641(10)	0.029(2)
O4	0.1982(9)	0.3854(10)	−0.0486(9)	0.032(2)

and, therefore, were partly translucent, still well shaped, pale yellow pyramids with dimensions $0.36 \times 0.26 \times 0.24 \text{ mm}^3$. Structure refinement was performed using SHELXL97 software.²⁹ The final *R*-factor (Table 1) is higher than usual, because of the rather low crystallinity and, therefore, broader than usual diffraction peaks.

Powder Pattern Indexing. Both single crystal and powder data had to be used to solve the crystal structure of the monoclinic anhydrous phosphate **C** because of the relatively low crystallinity of the crystals and the heavily overlapping peaks on the powder pattern. Crystals were split, hexagonally shaped prisms. A full reciprocal sphere experiment yielded about 20 broad peaks (all at low angles), which allowed the determination of the lattice, with dimensions 5.5, 7.5, and 8 Å. A reasonable quality powder diffraction pattern was collected by using Mo K α radiation which improved the peak width. The best solution from ITO indexing³⁰ had 19 of 20 lines indexed and gave a monoclinic cell with dimensions agreeing with the single crystal data.

Solving Structure C from Powder Data. Rietveld refinement of a structure based on the atomic coordinates of **A** (except for the water) did not converge to any reasonable model. Therefore models were generated initially using AlPO_4 , which has the same oxidation state and is known to form similar compounds. The first model was treated with Dmol3 and CASTEP routines from Materials Studio³¹ applying geometry optimization by the means of DFT (density functional theory), and the DMol3 geometry optimization converged in 16 cycles (24 h on 2 GHz PC) giving a model with a practically perfect AlO_4 tetrahedron with Al–O distance 1.75 Å.

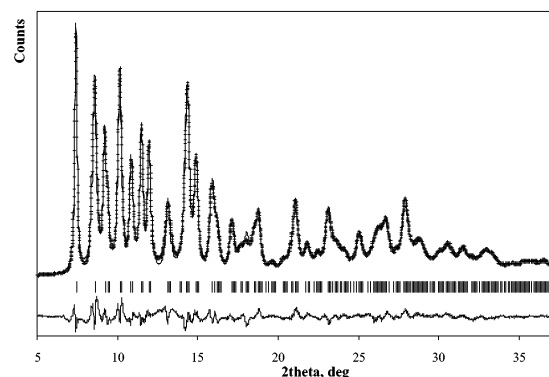


Figure 1. Rietveld refinement plot for monoclinic FePO_4 at 298 K, Mo K α radiation (observed, +; calculated, — (solid line); reflections, | (vertical lines); difference, bottom).

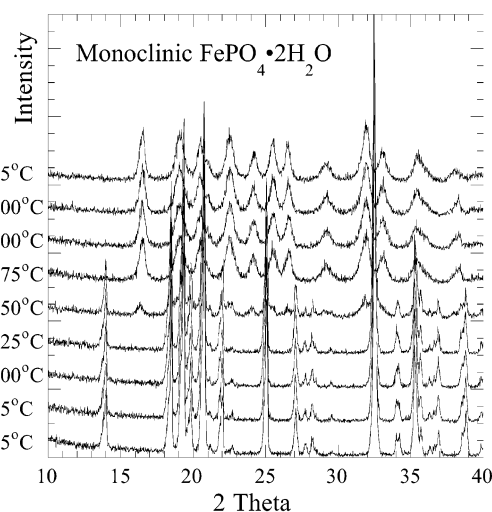


Figure 2. Powder XRD pattern of monoclinic $\text{FePO}_4 \cdot 2\text{H}_2\text{O}$ at different temperatures, Cu K α radiation.

Subsequently, applying DMol3 geometry optimization to tetrahedral model for FePO_4 yielded a deformation of the tetrahedron, increasing the Fe coordination number from 4 to 5 with the coordination polyhedron being square pyramid. A second model based on the coordinates of **A** was treated with a purely geometrical approach, the distance least-square method realized in DLS-76.³² This also rapidly converged and was practically the same as the first model except for differences in the Al–O and Fe–O distances.

The final Rietveld refinement, conducted using the GSAS/EXPGUI system,^{33,34} resulted in the deformation of the Fe tetrahedron into a trigonal bipyramid, while the PO_4 tetrahedra were maintained without significant changes. The refinement results are provided in Tables 1 and 2; the difference plot is shown in Figure 1.

Results and Discussion

XRD and Thermal Analysis. The powder X-ray pattern of the hydrothermally formed dihydrate of formula $\text{FePO}_4 \cdot 2\text{H}_2\text{O}$ showed a mixture of the phosphosiderite and strengite

(29) Sheldrick, G. M. *SHELXL-97*; University of Göttingen: Göttingen Germany, 1997.

(30) Visser, J. W. *J. Appl. Crystallogr.* **1969**, 2, 89–95.

(31) *Materials Studio*; Accelrys Inc.: San Diego, CA, 2001.

(32) Baerlocher, Ch.; Hepp, A.; Meier, W. M. *DLS-76, a Program for the Simulation of Crystal Structures by Geometric Refinement*; Institute of Crystallography and Petrography, ETH: Zurich, Switzerland, 1997.

(33) Larsen, C. A.; Von Dreele, R. B. *GSAS: General Structure Analysis System*; LANL: Los Alamos, NM, 1990.

(34) Toby, B. *EXPGUI. A Graphical User Interface for GSAS*; NIST Center for Neutron Research: Gaithersburg, MD, 2001.

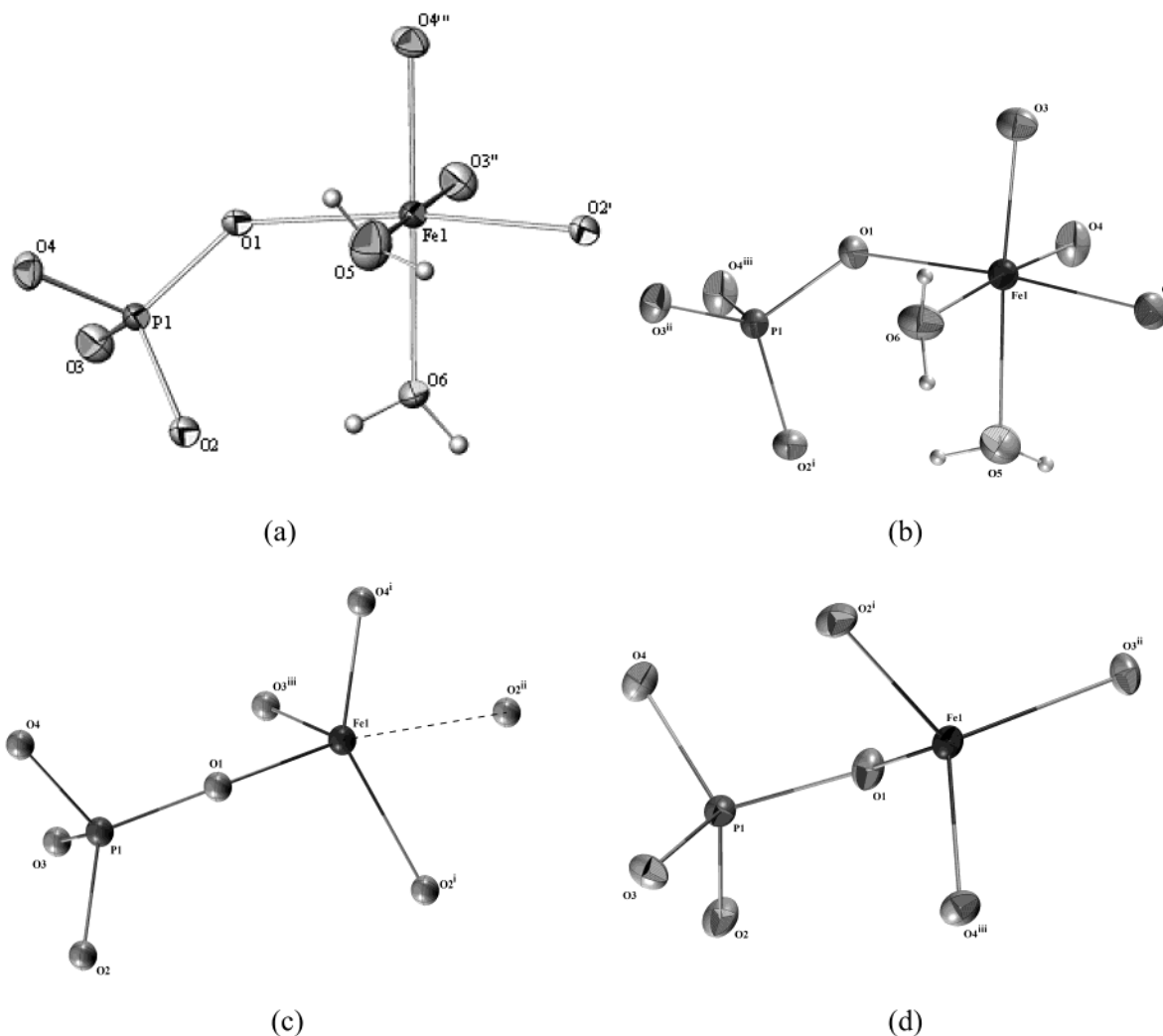


Figure 3. Ellipsoid plots and labeling of (a) monoclinic $\text{FePO}_4 \cdot 2\text{H}_2\text{O}$, (b) orthorhombic $\text{FePO}_4 \cdot 2\text{H}_2\text{O}$, (c) monoclinic FePO_4 , and (d) orthorhombic FePO_4 . Dashed line shows the longer fifth Fe—O bond in (c); (c) was refined using powder data and isotropic parameters.

phases. Gravimetric thermal analyses for both phosphates are similar, showing just one sharp peak with a weight loss of $\sim 19.1\%$ in the range $120\text{--}180\text{ }^\circ\text{C}$, which is due to the dehydration reaction. This agrees well with the calculated value of 19.3% for $\text{FePO}_4 \cdot 2\text{H}_2\text{O}$. The change of the X-ray pattern during dehydration is shown in Figure 2 for the monoclinic form of $\text{FePO}_4 \cdot 2\text{H}_2\text{O}$. The powder X-ray diffraction patterns show that the dehydration has started by $150\text{ }^\circ\text{C}$ and is complete by $175\text{ }^\circ\text{C}$, in agreement with the TGA data. The data in Figure 2 also show that the structure is still stable at $400\text{ }^\circ\text{C}$. At higher temperatures, it will convert to the quartz-type structure verlinite; these phase transitions are not reversible. Rehydration does not occur on immersion in water.

Structure Descriptions. The structures of the two hydrates, monoclinic **A** and orthorhombic **B**, are built up from Fe octahedra (Figure 3a,b and Table 2) and PO_4 tetrahedra sharing corners to form 3D frameworks as shown in Figure 4a,b. There is no edge or face sharing of the polyhedra in these structures. Each Fe octahedron share corners with four P tetrahedra, and the remaining two corners are occupied by two water molecules (O5 and O6). Each PO_4 tetrahedron, in its turn, shares four corners with four FeO_6 octahedra

(Figure 4a,b). This redetermination of their structures using single crystal data allowed the location of the positions of the H-atoms that make a branched system of H-bonds.

Both of the described dihydrate compounds, **A** and **B**, easily lose water on heating and/or under vacuum resulting in two new anhydrous iron phosphates, FePO_4 **C** and **D**. They crystallize in the same space group as their corresponding hydrates **A** and **B**. The structural determinations show that their frameworks are the same as those in the parent hydrates. The only bonds that are lost on dehydration are the coordination Fe—O bonds from the oxygens in the water molecules and the H-bonds formed by the two water molecules. Thus, the coordination of the Fe becomes tetrahedral because of the loss of 2 water molecules. However, in **C**, the Fe tetrahedron is somewhat distorted because of an additional weak $\text{Fe} \cdots \text{O2}^{\text{ii}}$ bond, which is 2.24 \AA in length (Table 3) and dotted in Figure 3c. This fifth atom makes a trigonal bipyramid around each Fe atom. However, the Fe coordination polyhedra in **C** can be interpreted either as trigonal bipyramids or as tetrahedra. The latter is used in Figure 4c for simplicity and clarity.

During dehydration, the monoclinic lattice (**A** \rightarrow **C**) shrinks as much as 27% , while the volume of the orthor-

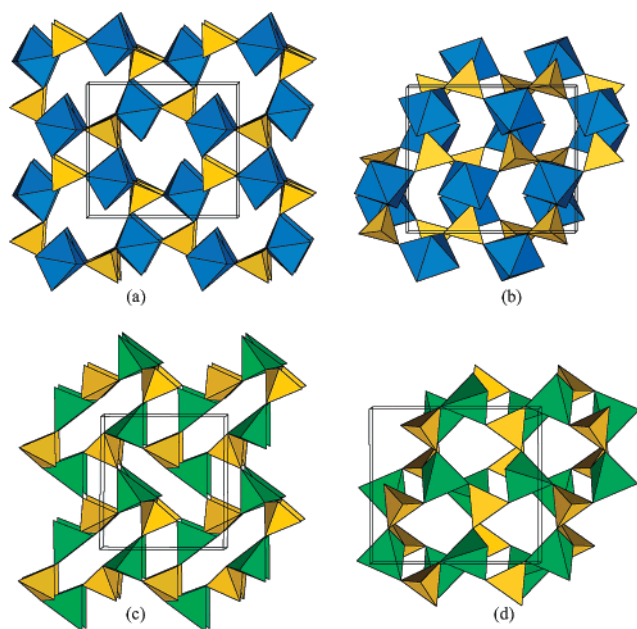


Figure 4. Polyhedral representation of the structure of monoclinic (a) $\text{FePO}_4 \cdot 2\text{H}_2\text{O}$, (b) orthorhombic $\text{FePO}_4 \cdot 2\text{H}_2\text{O}$, (c) monoclinic FePO_4 with Fe shown as tetrahedra, and (d) orthorhombic FePO_4 . Blue corresponds to FeO_6 octahedra in hydrated phosphates, green corresponds to FeO_4 tetrahedra in anhydrous phosphates, and yellow corresponds to PO_4 groups. All structures are shown along a axis, b axis across, c axis up.

Table 3. Selected Distances (Å) and Angles (deg) for Compounds **A–D**^a

A, Monoclinic $\text{FePO}_4 \cdot 2\text{H}_2\text{O}$		B, Orthorhombic $\text{FePO}_4 \cdot 2\text{H}_2\text{O}$	
Fe1–O3	1.944(3)	Fe1–O3	1.948(1)
Fe1–O4	1.950(3)	Fe1–O4	1.950(2)
Fe1–O2	1.974(4)	Fe1–O2	1.983(2)
Fe1–O1	1.977(3)	Fe1–O1	1.990(1)
Fe1–O6	2.012(4)	Fe1–O6	2.041(2)
Fe1–O5	2.070(4)	Fe1–O5	2.105(2)
O2–Fe1–O1	170.5(2)	O2–Fe1–O1	174.80(6)
O3–Fe1–O5	177.8(2)	O3–Fe1–O5	170.84(6)
O4–Fe1–O6	176.0(2)	O4–Fe1–O6	172.92(6)
C, Monoclinic FePO_4		D, Orthorhombic FePO_4	
Fe1–O4	1.809(9)	Fe1–O2	1.838(8)
Fe1–O1	1.864(9)	Fe1–O3	1.839(8)
Fe1–O3	1.867(9)	Fe1–O4	1.843(9)
Fe1–O2	1.965(10)	Fe1–O1	1.875(9)
Fe1–O2''	2.239(9)		
O1–Fe1–O2''	169.5(4)	O2–Fe1–O3	111.8(4)
O4–Fe1–O3	109.5(4)	O2–Fe1–O4	109.7(4)
O4–Fe1–O2	123.6(4)	O3–Fe1–O4	108.0(4)
O3–Fe1–O2	124.9(4)	O2–Fe1–O1	107.8(4)
		O3–Fe1–O1	108.4(4)
		O4–Fe1–O1	111.2(4)

^a For octahedra (**A** and **B**), only angles between opposite bonds are shown, for trigonal bipyramid (**C**), those between apical bonds and bonds forming the base are shown, and for tetrahedra (**D**), all are shown.

hombic lattice (**B** → **D**) shrinks just 13%. This indicates that the monoclinic lattice undergoes substantially greater deformation than the orthorhombic one, and it is in good agreement with the appearance of the additional bond discussed previously. The degree of deformation is not so obvious from the polyhedral representation of Figure 4, but it can be clearly seen in Figure 5. Both anhydrous compounds **C** and **D** have the same connectivity in the first and second coordination spheres. Each Fe tetrahedron shares 4 corners with 4 P tetrahedra, and vice versa, each P tetrahedron shares

4 corners with 4 Fe tetrahedra (Figure 4c,d), the same way as in the corresponding **A** and **B** hydrates. Thus, a more complex analysis is needed to describe the difference between **C** and **D** and their interrelation with other compounds.

These structures can be better understood by considering their backbone frameworks. These can be considered either using $4 \cdot 8^2$ layers or using hexagonal 6^3 layers. The backbone connectivity, using $4 \cdot 8^2$ layers, is illustrated in Figure 5, where Fe–O–P binding is represented by the Fe–P line. This figure shows the difference between the orthorhombic and monoclinic modifications of anhydrous as well as hydrous iron phosphates. It also reveals the identical connectivity of the layer in both modifications, where 8-member rings and 4-member rings share edges to form a $4 \cdot 8^2$ Kármán net. The 3D framework is defined by the sequence of interlayer connectivity of the four-member ring, marking links up (U) and down (D) the layer. Again, in both monoclinic and orthorhombic cases, the connectivity of each square is UDD. However, the position of each other layer is different as shown in Figure 5. In the orthorhombic structures, the 8-member and 4-member rings alternate, while in monoclinic structures they coincide. From this, it is clear that the monoclinic structure can shrink much more than the orthorhombic one, because the 8-member rings form empty tunnels that are easily deformed. This deformation is so strong that weak bonds Fe–O2 (dotted lines in Figure 5d) are formed across the 8-member rings (Table 3).

Representing FePO_4 frameworks with $4 \cdot 8^2$ nets reveals their relationship with the AlPO_4 zeolites described in ref 35. AlPO_4 -C and AlPO_4 -D nets have a connectivity identical to that described here. However, their interlayer connectivity is quite different. The 4-member ring sequence is UDD for AlPO_4 -D and UDUD for AlPO_4 -C. In the case of FePO_4 , the rings in adjacent layers are perfectly aligned and form regular (in **C**) or just slightly deformed (in **D**) octagonal tunnels. Interestingly, AlPO_4 also forms monoclinic³⁶ and orthorhombic³⁷ dihydrates that are isostructural to the corresponding iron compounds **A** and **B**.

The backbone frameworks can also be described using hexagonal 6^3 layers as shown in Figure 6a,b. The interlayer connectivity can be identified by a sequence of hexagons linked up and down, which is UUDUD for monoclinic phosphate and UDDUD for the orthorhombic one. Note that the sphalerite and wurtzite structures can be described in the same way with UDUDUD sequence and they differ by relative placement of adjacent layers.

Hexagonal layers are also found in another FePO_4 modification (**E**), which crystallizes in the orthorhombic system, space group $Pnma$, $a = 9.8142(2)$ Å, $b = 5.7893(2)$ Å, $c = 4.7820(2)$ Å.¹⁰ This compound is obtained from LiFePO_4 by Li deintercalation. Structure **E** differs from the other iron phosphates by the octahedral coordination of the

(35) Keller, E. B.; Meier, W. M. *Solid State Ionics* **1990**, *43*, 93–102.

(36) Kniep, R.; Mootz, D.; Vegas, A. *Acta Crystallogr.* **1973**, *B29*, 2292–2294.

(37) Kniep, R.; Mootz, D.; Vegas, A. *Acta Crystallogr.* **1977**, *B33*, 263–265.

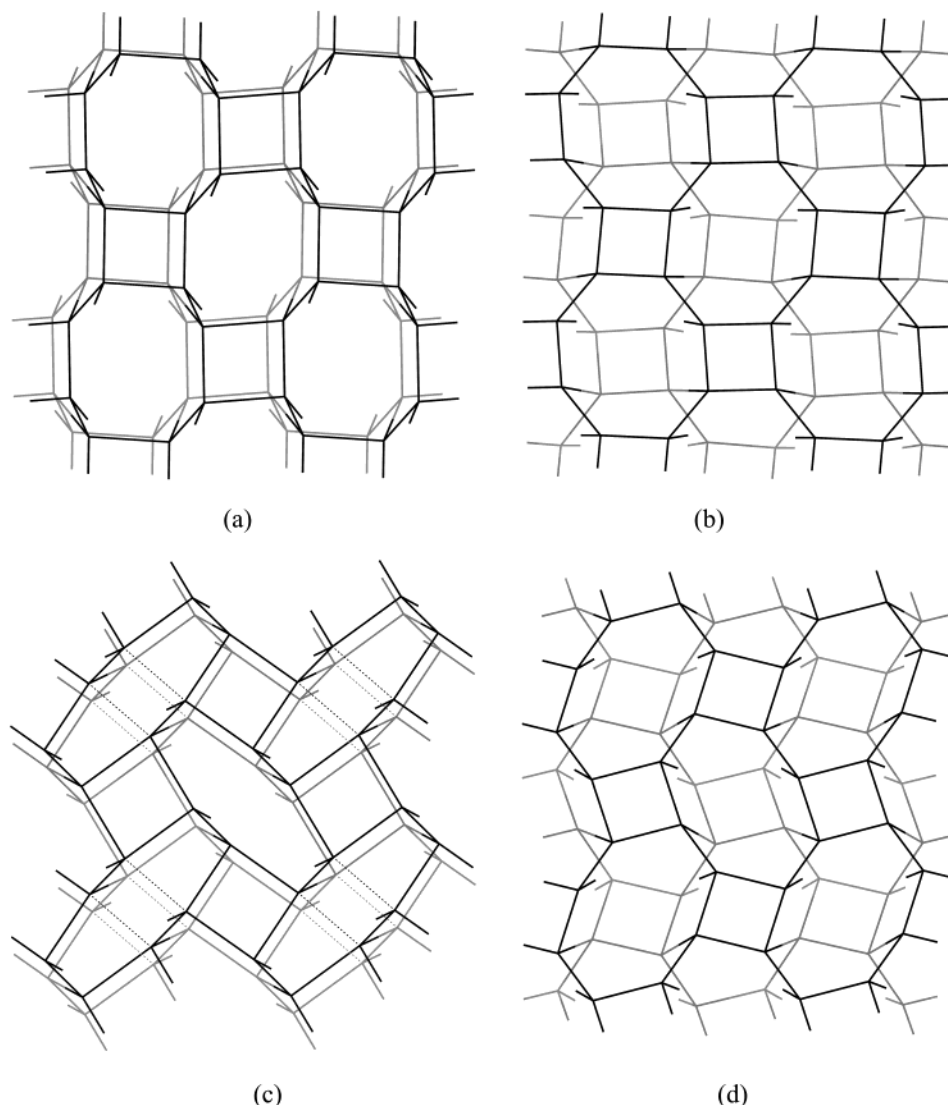


Figure 5. Two layers of the Fe–P backbone framework for (a) monoclinic $\text{FePO}_4 \cdot 2\text{H}_2\text{O}$ along the c axis, (b) orthorhombic $\text{FePO}_4 \cdot 2\text{H}_2\text{O}$ along the a axis, (c) monoclinic FePO_4 along the a axis, (d) and orthorhombic FePO_4 along the a axis. Darker line corresponds to the top layer; lighter line corresponds to the bottom layer.

Fe atom, leading to different connectivity in the backbone framework. Figure 6c depicts these interconnected hexagonal layers. Here, in contrast to structures with tetrahedrally coordinated metal, each corner is linked to both upper and lower layers. Thus, this structure is much more dense than the other anhydrous phosphates (Table 4, phases **C–F**) and can be easily converted to either **C** or **D** by breaking links between layers in specific order so that each corner is bound to either the upper or lower layer but only once.

Both compounds **C** and **D** are metastable and convert irreversibly into trigonal FePO_4 (**F**), when heated above 450 °C. Trigonal FePO_4 has the α -quartz-type structure³⁸ with essentially the same connectivity in the first and second coordination spheres as that of **C** and **D**. The Fe coordination is tetrahedral with Fe–O in the range 1.85–1.86 Å. Nevertheless, its backbone framework has a different configuration from the **C** and **D** phosphates and cannot be

described using either $4 \cdot 8^2$ or 6^3 layers. As can be seen from Figure 6, alternating Fe and P tetrahedra form a helical chain spiraling around the 3_1 screw axis. These chains are arranged in a 3D framework forming hexagonal-like tunnels.

Another known FePO_4 phase, the high pressure⁸ modification of FePO_4 (**G**), has Fe in octahedral coordination, as in **E**. However, these octahedra share opposite edges with each other to form a chain. The PO_4 tetrahedra share corners with the Fe octahedra linking those chains into a 3D framework. Hence, each corner is shared by two Fe octahedra and one PO_4 tetrahedra. Thus, this structure is quite different from all other iron phosphates and has the highest density (Table 4).

When comparing structures of the new iron phosphates with other chemically similar classes of compounds, it was found that FeAsO_4 (**H**) (space group $P2_1/n$, $a = 7.560(1)$ Å, $b = 8.081(1)$ Å, $c = 5.012(1)$ Å, $\beta = 104.42(1)^\circ$)³⁹ is similar

(38) Goiffon, A.; Dumas, J.-C.; Pjillipot, E. *Rev. Chim. Miner.* **1986**, 23, 99.

(39) Reiff, W. M.; Kwiecien, M. J.; Jakeman, R. J. B.; Cheetham, A. K.; Torardi, C. C. *J. Solid State Chem.* **1993**, 107, 401–412.

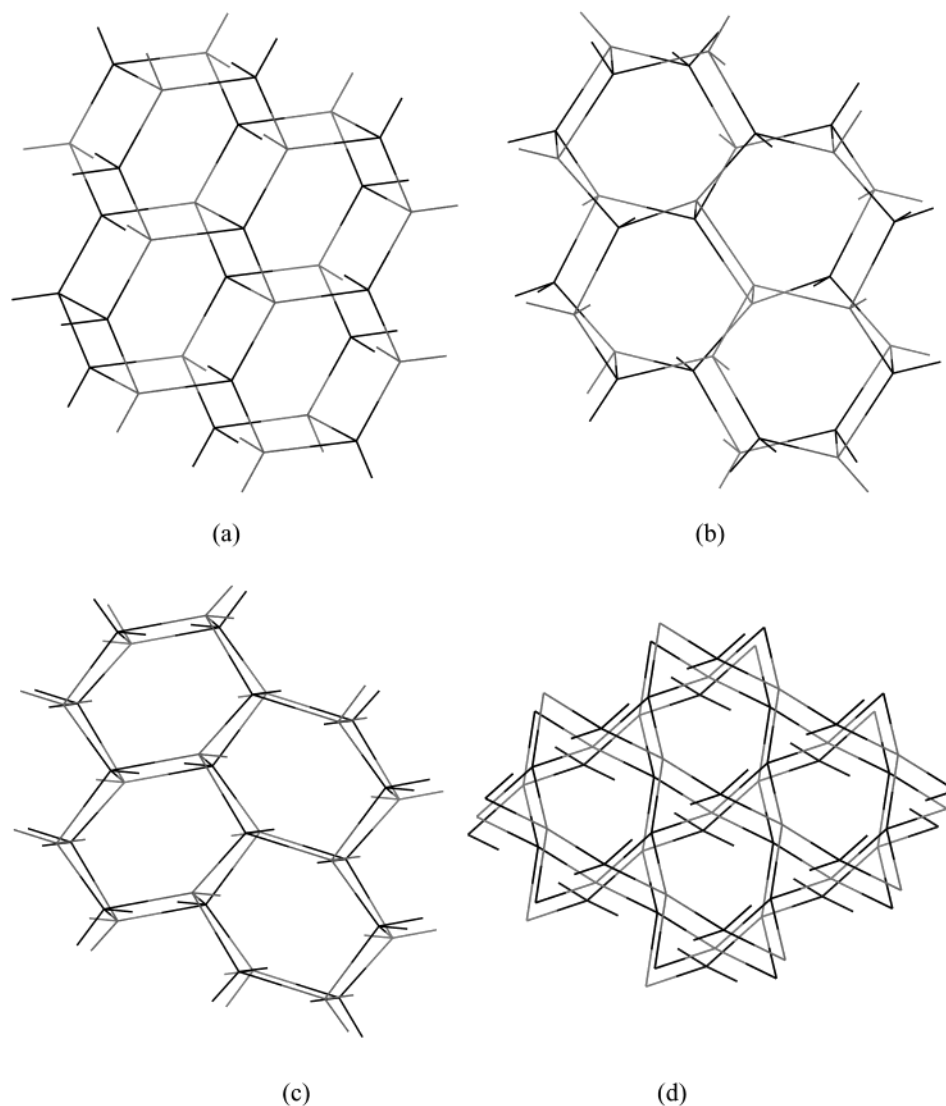


Figure 6. Backbone framework of (a) monoclinic FePO_4 along the b axis, (b) orthorhombic FePO_4 along the a axis, (c) FePO_4 from lithium extraction along the a axis, (d) α -quartz FePO_4 along the c axis. Darker line corresponds to the Fe–O bond; lighter line corresponds to the P–O bond.

Table 4. Volume and Density of the Iron Phosphate Phases

FePO_4 phase	volume/ FePO_4 (\AA^3)	density (g/cm^3)
A monoclinic hydrate	112.3	2.763
B orthorhombic hydrate	108.4	2.862
C monoclinic	82.1	3.049
D orthorhombic	94.0	2.663
E orthorhombic ¹⁰	67.9	3.689
F trigonal ⁷	82.0	3.056
G high-pressure FePO_4 ⁸	64.2	3.902
H FeAsO_4 ³⁹	74.1	4.362/3.378 ^a

^a Density recalculated for FePO_4 .

in structure to **C**, the monoclinic FePO_4 . The coordination polyhedron of Fe in **H** is also a distorted trigonal bipyramid but slightly different. In **C**, the bipyramid is significantly distorted, and the longest Fe–O (2.24 \AA) lies across the 8-member ring as shown in Figure 7, while in **H** the second longest bond (2.01 \AA) lies across the ring (the longest is 2.06 \AA). Other Fe–O bonds are between 1.88 and 1.91 \AA . Note that the volume is about 10% less for **H** than for **C**, which is probably due to the stronger Fe–O interaction

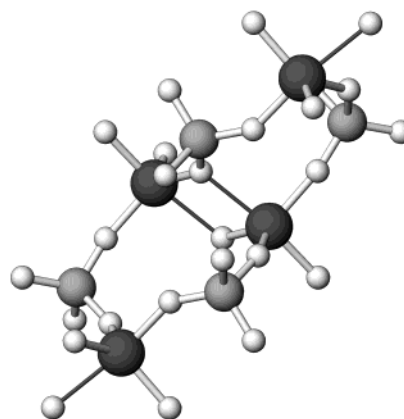


Figure 7. Structure of FePO_4 (**C**) with the trigonal pyramidal iron coordination showing the elongated bonds as thin gray lines. The Fe and P atoms are shown as the dark gray and light gray bigger balls, respectively.

across the 8-member ring, where the bond length is 2.01 \AA in **H** versus 2.26 \AA in **C**.

The volume per formula unit and calculated density are given in Table 4. The orthorhombic **D** phase is the most

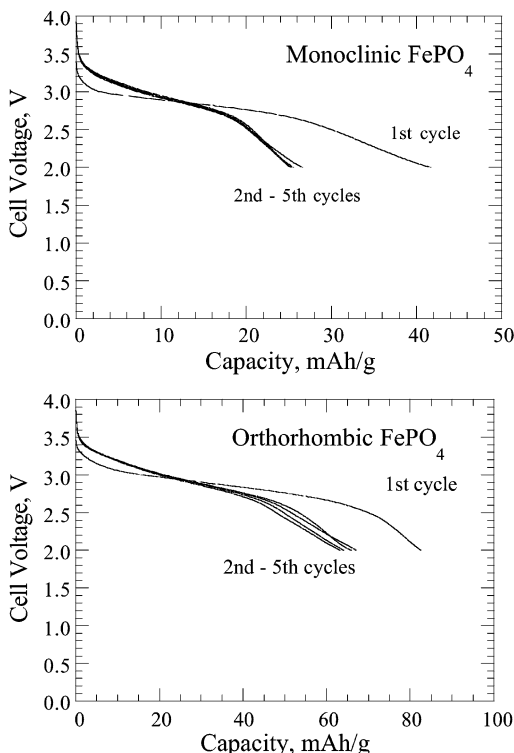


Figure 8. Electrochemical lithium intercalation, at 0.2 mA/cm² between 4 and 2 V, into monoclinic FePO₄ (top) and orthorhombic FePO₄ (bottom). 170 mAh/g = 1 Li/FePO₄.

open framework among the iron phosphates and arsenate. The monoclinic **C** is as dense as the trigonal FePO₄. Interestingly, the monoclinic arsenate **H** has a volume/formula unit about 10% less than **C**. Orthorhombic FePO₄, formed by lithiation of LiFePO₄, has a noticeably higher density than the others.

Electrochemical Properties. The insertion of lithium was followed by measuring the voltage of an electrochemical cell comprising a lithium anode and the ferric phosphate as cathode; the data are shown for the anhydrous monoclinic and orthorhombic iron phosphates in Figure 8. The lithium insertion is rather low in both cases, where insertion of one lithium ion corresponds to 170 mAh/g. The orthorhombic phase has the higher capacity incorporating 0.5 Li per FePO₄, whereas the monoclinic phase incorporates only half that amount. These results can be compared to those of amorphous FePO₄⁴ and the heterosite FePO₄⁹ where, respectively, 0.8 and close to 1 lithium ion can be reversibly incorporated. These differences are almost certainly associated with the coordination of the redox active iron atom. In the heterosite form, the iron is octahedrally coordinated, which is a stable environment for both the ferrous and ferric states in oxides. In contrast, in the two compounds reported here, the ferric ion has a coordination of four and five. In the latter, the monoclinic form, the smaller capacity may be associated with the Fe–O–Fe bonding across the tunnel, which will impede the diffusion of lithium ions. In the trigonal quartz form, where the iron is strictly tetrahedral, there is little redox behavior.⁴ This can be associated with the instability of tetrahedral ferrous ions, so that for iron reduction to occur reorganization of the oxygen lattice must occur to increase

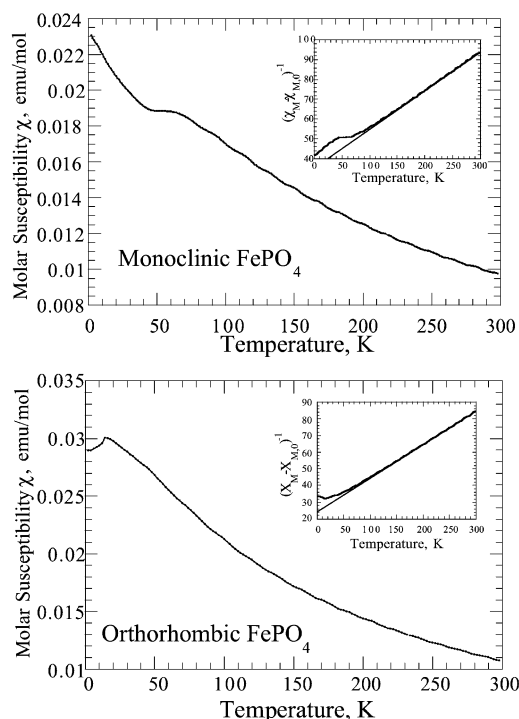


Figure 9. Molar magnetic susceptibility vs temperature for (top) monoclinic FePO₄ and (bottom) orthorhombic FePO₄ in the 2–298 K range at a magnetic field of 1000 Oe.

the coordination number of the iron atoms. The Giniite iron phosphate phase, Fe_{5–x}(PO₄)₂(HPO₄)₂(OH)₄, where iron is found in octahedral coordination, exhibits complete reversibility of 1 Li/Fe.⁴⁰ This behavior has also been observed for vanadium, where tetrahedral vanadium(V) is electrochemically inactive, in contrast to five- or six-coordinate vanadium.⁴¹ The amorphous FePO₄ presumably has some approximately six-coordinate iron atoms as it exhibits behavior intermediate between these new compounds and the crystalline octahedral heterosite material.

Magnetic Properties. The molar magnetic susceptibility of these two phosphates is shown in Figure 9. At temperatures above 80 K, the Curie–Weiss law is satisfied. By 3-parameter nonlinear square root fitting for $\chi = \chi^\circ + C/(T - \Theta)$ of the curves above 200 K, it is found that the effective magnetic moment for the monoclinic phosphate is 6.392 μ_B , and for the orthorhombic phosphate, 6.305 μ_B . This is a little bit higher than the theoretical data for spin-only high spin iron(III), 5.916 μ_B . Θ is equal to –179.8 and –120.1 K for the monoclinic and orthorhombic phosphate, respectively, indicating antiferromagnetic interactions in these two compounds at low temperatures. These values compare with the values of 5.60 μ_B and $\Theta = -84$ K and 6.02 μ_B and $\Theta = -128$ K for the trigonal and CrVO₄-type FePO₄.⁸ The stronger interactions with a higher $|\Theta|$ in the monoclinic phosphate can be attributed to the existence of Fe–O–Fe bonding in this phase. In the orthorhombic phase, there is no Fe–O–Fe bonding, only Fe–O–P–O–Fe bonding. The Fe–Fe interactions are even stronger in FeAsO₄, where Θ

(40) Song, Y.; Zavalij, P. Y.; Whittingham, M. S. To be published.

(41) Chirayil, T. A.; Zavalij, P. Y.; Whittingham, M. S. *Chem. Mater.* **1998**, *10*, 2629–2640.

has a value of -231 K ;³⁹ here, the Fe—O bond is only 2.01 Å compared to 2.24 Å in the phosphate. The orthorhombic phosphate shows a magnetic phase transition at ca. 15 K (the Néel point), where it begins to order antiferromagnetically. This is similar to the quartz phase of iron phosphate, which shows a spin-reorientation transition at ca. 17 K .¹² In addition, the high value of the $|\Theta/T_N|$ ratio suggests the presence of magnetic frustration in both phosphates. The shoulder observed around 50 K for **C** might be due to the appearance of antiferromagnetic short-range ordering.

Conclusions

Monoclinic and orthorhombic ferric phosphate dihydrate lose their water by a topotactic reaction, with only the iron water bonds being broken in addition to the hydrogen bonding. This results in the iron coordination being reduced from octahedral to distorted tetrahedral. The monoclinic form has a fifth oxygen at 2.24 Å , with the other Fe—O distances varying from 1.81 to 1.96 Å . The Fe—O tetrahedron in the orthorhombic form is more regular with all the Fe—O bonds falling in the range 1.84 – 1.88 Å . Both of these FePO_4 phases exhibit Curie–Weiss behavior above 80 K , with antiferro-

magnetic interactions at lower temperatures. These interactions are stronger in the monoclinic phase where there is Fe—O—Fe bonding. Both phases can be partially reduced by lithium ions and are intermediate in behavior between the inactive trigonal phase and the active heterosite phase that contains FeO_6 octahedra.

Acknowledgment. We thank our colleagues Professor David Jenkins, for help with the high temperature X-ray measurements, and Dr. Vitalij K. Pecharsky (Iowa State University, Ames), for the Rigaku powder diffraction data. Financial support by the National Science Foundation, Grant DMR 9810198, is greatly appreciated.

Supporting Information Available: Table of indexed powder pattern containing hkl , observed and calculated 2θ , d spacing, and relative intensities of reflections for compound **C**. Table of H-bonds for compounds **A** and **B**. Complete crystallographic, experimental, and structural data for compounds **A**, **B**, **C**, and **D** in CIF format. This material is available free of charge via the Internet at <http://pubs.acs.org>.

IC025688Q